# Adaptive Maximization of the Harvested Power for Wearable or Implantable Sensors With Coulomb Force Parametric Generators

Masoud Roudneshin, *Member, IEEE*, Kamran Sayrafian, *Senior Member, IEEE*, and Amir G. Aghdam, *Fellow, IEEE*

***Abstract*—Miniaturized wearable or implantable medical sensors (or actuators) are often used in the Internet of Things (IoT) technologies in healthcare applications. However, their limited source of power is becoming a bottleneck for the pervasive use of these devices, especially, as their functionality increases. Kinetic-based micro-energy harvesters can generate power through the natural human body motion. Therefore, they can be an attractive solution to supplement the source of power in medical wearables or implants. The architecture based on the Coulomb force parametric generator (CFPG) is the most viable micro-harvester solution for generating power from human motion. This article proposes three methods: a linear estimation approach, a multi-armed bandit algorithm, and a min–max-based approach to adaptively estimate the desirable electrostatic force in a CFPG using the input acceleration waveform. Through extensive simulations, the performance of the proposed methods in maximizing the output power of the micro-harvester is evaluated.**

***Index Terms*—Coulomb force parametric generator (CFPG), Internet of Things (IoT) in healthcare, low power wearable sensors, micro-energy harvesting, online optimization.**

## I. Introduction

Energy harvesting (EH) is the process of capturing energy from the ambient environment and converting it into electrical energy. Different sources for EH include solar, wind, thermal, and kinetic energy. Micro-energy harvesters refer to a class of miniaturized EH devices that can generate electrical power for small-scale and low-power sensors and actuators [1], [2]. These, typically low-power, devices are critical components of the Internet of Things (IoT) technology. As interface elements with physical objects, low-power sensors and actuators often rely on small batteries to operate and reliably exchange information between the object and the Internet. By reducing the frequency of battery replacement or recharge, micro-energy harvester offers a prolonged operational lifetime or possibly self-sustainability for the IoT sensors and actuators. Integration and co-design of micro-energy harvesters with the sensor architecture (conceptually shown in Fig. 1) has the potential to accelerate the development of green technology that positively impacts the environment. Therefore, micro-energy harvester is regarded as one of the key enabling technologies that can empower further development and expansion of IoT in smart homes and appliances, electric vehicles, and, in particular, wearable sensors and implants, which are the main focus of this work.

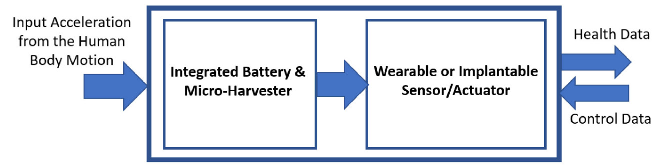


Fig. 1. Conceptual diagram of integrated micro-energy harvester and low-power wearable/implant sensor.

Kinetic-based micro-energy harvester is considered to be a promising technology for small wearable or implantable devices [2], [3], [4], [10], [11], [12], [13]. As the nature of their applications necessitates, these small devices are typically expected to operate for long periods of time without interruptions. This is especially the case for medical implants. Large batteries or frequent recharge might not be feasible for these devices, particularly when connection to IoT-health infrastructure further increases their energy consumption. Conversion of the kinetic energy into electrical energy can be achived through magnetic, piezoelectric and electrostatic forces. Compared to the first two, the electrostatic-based conversion is much more effective in micro scales [14]. Therefore, this approach allows for further miniaturization of the harvester's size, making it more favorable for very small wearable or implantable medical sensors.

The Coulomb force parametric generator (CFPG) is a kinetic-based micro-energy harvester that can best harvest

Manuscript received 21 March 2023; accepted 11 April 2023. Date of publication 25 April 2023; date of current version 25 September 2023. This work was supported by the National Institute of Standard and Technology (NIST) under Grant 60NANB20D163. *(Corresponding author: Amir G. Aghdam.)*

This work involved human subjects or animals in its research. Approval of all ethical and experimental procedures and protocols was granted by Concordia University under Application No. 30013664 and NIST under Application No. ITL-2021-0273.

Masoud Roudneshin was with the Department of Electrical and Computer Engineering, Concordia University, Montreal, QC H4B 1R6, Canada. He is now with Traxara Robotics, Montreal, QC, Canada (e-mail: masoud.roudneshin@concordia.ca; amir.aghdam@concordia.ca).

Masoud Roudneshin and Amir G. Aghdam are with the Department of Electrical and Computer Engineering, Concordia University, Montreal, QC H4B 1R6, Canada (e-mail: masoud.roudneshin@concordia.ca; amir.aghdam@concordia.ca).

Kamran Sayrafian is with the National Institute of Standards and Technology, Gaithersburg, MD 20899 USA (e-mail: kamran.sayrafian@nist.gov).

Digital Object Identifier 10.1109/JIOT.2023.3269953

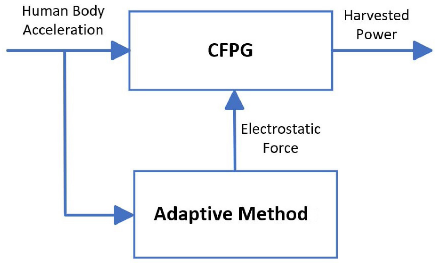


Fig. 2. Schematic of a CFPG using adaptive electrostatic force.

energy from low-frequency nonstationary movements [14], [15], [16], [17]. For acceleration waveforms consisting of only a single harmonic, resonant-based micro-harvesters can perform optimally. By using the optimal parameters, those micro-generators can harvest the maximum amount of power at their operating frequency. However, the acceleration resulting from the human body motion is not a simple sinusoidal waveform and consists of a rich spectral content. For such motions, a CFPG is proven to extract the maximum amount of power; and therefore, considered to be the most suitable architecture for wearables or implants. The core component of a CFPG includes a proof mass that can move between two plates. An internal electrostatic force maintained by a transducer holds the proof mass to one of the plates. The proof mass stays attached to the plate until the input acceleration due to the movement of the human body overcomes this holding force. Then, the proof mass is detached and moves toward the other plate. Energy is generated only if the proof mass makes a full flight (i.e., reaches the other plate) against the direction of the electrostatic holding force. If the proof mass fails to make a full flight, the amount of the extracted energy during its flight is dissipated when it returns to its initial position. After each full flight, the direction of the holding force applied to the proof mass reverses, and the EH process continues accordingly.

Typically, the magnitude of the holding force is kept constant during this process. However, Budic et al. [18], Yarkony et al. [19], and Dadfarnia et al. [20] demonstrated that judicious adjustment of the holding force could significantly increase the output harvested power. The possibility of this adjustment to harvest the maximum amount of energy is especially important for wearable and implantable devices where a limited supply of energy is a critical bottleneck to their usability as well as improvement in future functionality. This concept is schematically shown in Fig. 2. For any input acceleration waveform, the adaptive methodology estimates the electrostatic force that maximizes the harvested power in a CFPG.

Budic et al. [18] investigated the output harvested power of a CFPG for different constant values of the holding force and daily activities. Through statistical analysis of the acceleration waveform generated by the human body movement, an upper bound on the harvested power of a CFPG device was obtained in [19]. Dadfarnia et al. [20] introduced a mathematical model for a more accurate estimation of the generated power by a CFPG. In addition, they formulated an adaptive optimization problem for adjusting the holding force with respect to the input acceleration waveform. The solution to this optimization problem is a mapping from the acceleration data in a given time interval to the optimal value of the holding force that should be used for the following time interval. As such, this type of adaptive adjustment of the holding force can be classified as an online (or dynamic) optimization problem. The underlying assumption in the proposed optimization is the temporal correlation in the acceleration waveform generated by the human body movement for sufficiently short time intervals. Roudneshin et al. [21], [23] proposed methodologies including machine learning approaches to solve this optimization problem and compared the harvested power for a limited number of acceleration waveforms.

In this article, we propose three methodologies to estimate the optimal value of the electrostatic holding force with relatively low computational power. First, by formulating a regularized optimization problem, we extend the linear estimation method proposed in [22] and [23] to enhance its generalizability to unobserved acceleration data and reduce overfitting with respect to the training data. Then, we investigate the applicability of a multi-armed bandit (MAB) algorithm to estimate the holding force using the history of the previously applied forces. In another approach, by considering the physical constraints of the proof mass, we propose an adaptive algorithm that estimates the holding force without the need for prior training with acceleration data. The contributions of this article can be summarized as follows.

1) Developing three adaptive methods to enhance the output power in a CFPG.
2) Evaluating the performance of the adaptive methodologies based on a comprehensive data set consisting of acceleration waveforms generated from various physical experiments.

The remainder of this article is organized as follows. In Section II, the problem formulation is described. We describe our adaptive approaches for estimating the holding force to maximize the harvested power in Section III. Section IV describes the data acquisition and calibration processes for the experiments. In Section V the impact of the so-called "decision set" and "decision interval" on the harvested power is studied, followed by a comparative performance evaluation in Section VI. Finally, conclusions and future directions are discussed in Section VII.

## II. Problem Formulation

In this section, a mathematical model for the CFPG is provided and an optimization problem for its output power maximization is introduced.

### A. CFPG Mathematical Model

Fig. 3 depicts the generic model of the core component of a CFPG, where a proof mass can move between two plates against the electrostatic holding force denoted by $F$. The proof mass is attached to either of the plates when the micro-generator is stationary or the external acceleration is not large enough. For sufficiently large external accelerations, the proof mass detaches from one plate and moves toward the other.

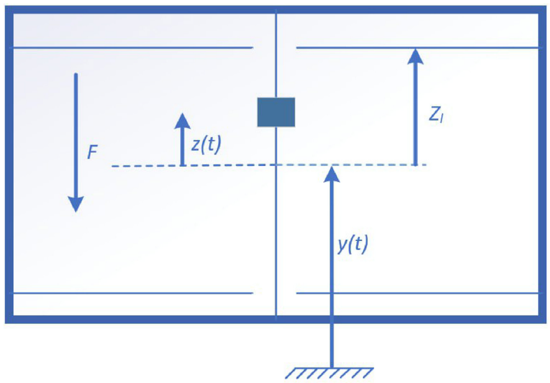


Fig. 3. Generic model of the core component in a CFPG.

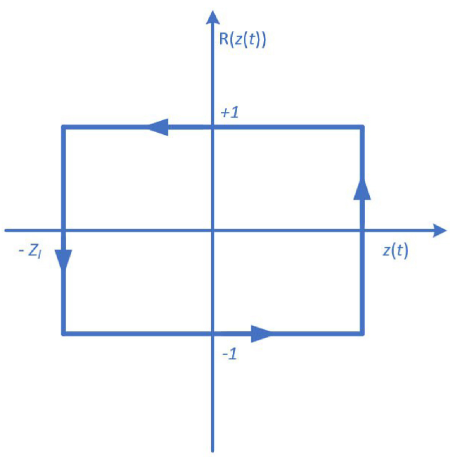


Fig. 4. Relay hysteresis function.

Once the proof mass completes a full journey between the two plates with separation of $2Z_l$, the work done against the electrostatic force is converted to electric energy. When the proof mass reaches the other plate, the direction of the holding force reverses and the energy conversion process continues.

Let the relative position of the proof mass with respect to the device's frame be denoted by $z(t)$. Also, denote by $y(t)$ the device motion with respect to the inertial frame. The following nonlinear differential equation models the dynamics of a CFPG as presented in [20]

$$m\ddot{y}(t) = -m\ddot{z}(t) + F \times \mathrm{R}(z(t)) \tag{1}$$

where $m$ denotes the mass, $\ddot{y}(t)$ is the acceleration with respect to the inertial frame, $\ddot{z}(t)$ is the relative acceleration of the proof mass with respect to the frame, and $F$ denotes the electrostatic force (also referred to as the holding force). The reversal of the holding force direction after a full flight of the proof mass is represented by a relay hysteresis function $R(\cdot)$ (see Fig. 4). The instantaneous power generated by the proof mass is given by

$$P(t) = F \times \dot{z}(t)$$

where $\dot{z}(t)$ is the relative velocity of the proof mass with respect to the frame.

*Remark 1:* As long as the proof mass moves in the opposite direction of the holding force, the instantaneous generated power has a positive value. If the proof mass cannot make a full flight, the motion direction reverses and the instantaneous power will turn negative. Once the proof mass returns to the starting plate, its motion results in a zero-average harvested power.

The average power generated in a CFPG is affected by several factors: the input acceleration, the distance between the two plates, the value of the proof mass, and the magnitude of the electrostatic force. In this article, assuming a constant size and geometry for the CFPG component shown in Fig. 3, the effect of the holding force on the generated power for various input acceleration will be investigated.

### B. Output Power Optimization

Assume that the holding force can be adjusted every $\Delta_i$ seconds. Then, at each time interval, the objective is to estimate the optimal holding force value which maximizes the average harvested power, i.e.,

$$\underset{F^{i+1,\Delta_i},\Delta_i}{\operatorname{argmax}} \left[ \frac{1}{\sum_{i=1}^{N} \Delta_i} \times \sum_{i=1}^{N} \int_{t_i-\Delta_i}^{t_i} P(t)dt \right] \tag{2}$$

where $\Delta_i$ is the optimal length of the $i$th decision interval, $F^{i+1,\Delta_i}$ is the optimal constant electrostatic force in the $(i+1)$th interval (as a function of $\Delta_i$), $N$ denotes the number of decision intervals and $P(t)$ is the instantaneous output power. Assume, for simplicity, that the length of the decision interval is fixed and denoted by $\Delta$. Then, (2) can be rewritten as

$$\underset{F^{i+1,\Delta}}{\operatorname{argmax}} \left[ \frac{1}{N\Delta} \times \sum_{i=1}^{N} \int_{t_0+(i-1)\Delta}^{t_0+i\Delta} P(t)dt \right]. \tag{3}$$

For a fixed decision interval $\Delta$, the optimal electrostatic force is a function of the acceleration waveform at the $i$th interval $[t_0 + (i-1)\Delta, t_0 + i\Delta]$. Hence, one way to estimate the holding force $F^{i+1,\Delta}$ is to employ a parametrized policy $\pi_{\boldsymbol{\theta}}$ such that

$$F^{i+1,\Delta} = \pi_{\boldsymbol{\theta}}\left(\ddot{\mathbf{y}}^i\right) \tag{4}$$

where $\boldsymbol{\theta}$ denotes a vector of parameters for the policy, and $\ddot{\mathbf{y}}^i \in \mathbb{R}^M$ denotes a vector of $M$ acceleration samples in the $i$th interval in (4).

It should be emphasized that the optimization problem (3) can be categorized as an online optimization since the knowledge of the future acceleration data is not required for the solution. In other words, $F^{i+1,\Delta}$ is estimated from the information in the $i$th interval (i.e., past acceleration data). For a known acceleration waveform, the maximum amount of the average harvested power can be obtained by an offline exhaustive search. Although this method cannot be utilized in practice, it provides an upper bound on the maximum achievable harvested power for the given acceleration waveform. For each decision interval $i$, the optimal value of the holding force can be obtained by the following offline optimization problem:

$$F^{\mathrm{opt},i} = \underset{F^{i,\Delta}\in\mathcal{F}}{\operatorname{argmax}} \left[ \frac{1}{N\Delta} \times \sum_{i=1}^{N} \int_{t_0+(i-1)\Delta}^{t_0+i\Delta} P(t)dt \right] \tag{5}$$

where $F^{\text{opt},i}$ denotes the optimal solution at each decision interval. We have used this method to assess the effectiveness of the proposed methods.

In practice, the range and resolution of the values of the estimated electrostatic forces that solve the online (or offline) optimization problems (3) [or (5)] are limited. Here, we consider a finite set of electrostatic forces $\mathcal{F}$ (hereafter referred to as the decision set) defined by

$$\mathcal{F} = \{F_i | F_{\min} \le F_i \le F_{\max}, F_i - F_{i-1} = \delta_F\} \tag{6}$$

where $F_{\min}$, $F_{\max}$, and $\delta_F$ denote the minimum, maximum and the increments for the holding force values. The impact of the decision set (i.e., $\mathcal{F}$) on the harvested power will be studied in Section V-A and V-B.

*Remark 2:* Let $E$ and $V$ denote the electrostatic field between the two plates and the operating voltage of a CFPG, respectively; then

$$E = \frac{V}{2Z_l}.$$

Also, let $q_{\text{mass}}$ denote the charge of the proof mass. The electrostatic force can then be formulated as

$$F = Eq_{\text{mass}} = \frac{V}{2Z_l} q_{\text{mass}}.$$

Given a decision set with components having fixed increments $\delta_F$, the proper range for the values of the electrostatic force is dependent on the technology that controls the supply voltage $V$. This must be taken into account for the practical implementation of a CFPG.

## III. Adaptive Methodologies

In this section, we describe our proposed methodologies that can adaptively estimate the electrostatic force to maximize the harvested power.

### A. Linear Estimation of the Holding Force

Consider that the holding force is estimated by a linear mapping from the absolute value of the acceleration data samples during the $i$th interval as

$$F^{\text{Lin},i} = \boldsymbol{\theta}^\intercal |\ddot{\mathbf{y}}|^{i-1}$$

where $\hat{F}^{\text{Lin},i}$ denotes the estimated holding force for the $i$th interval, and $\ddot{\boldsymbol{y}}^{i-1} \in \mathbb{R}^M$ is the acceleration vector from the $(i-1)$th interval, and $|.|$ denotes the absolute value operator. In addition, $\boldsymbol{\theta} \in \mathbb{R}^M$ is the vector of the linear estimator's parameters. To find the estimation parameters for the electrostatic force $\hat{F}^{\text{Lin},i}$, the average distance between the estimated and actual values of the holding force should be minimized. Therefore, the following minimization problem is formulated:

$$\underset{\boldsymbol{\theta}}{\text{minimize}} \quad \|\mathbf{F}^{\text{opt}} - \mathbf{F}^{\text{lin}}\| = \|\mathbf{F}^{\text{opt}} - \boldsymbol{\theta}^\intercal \ddot{\mathbf{Y}}\| \tag{7}$$

where $\mathbf{F}^{\text{opt}} = \{F^{\text{opt},i}\}_{i=1}^N$ and $\mathbf{F}^{\text{lin}} = \{\hat{F}^{\text{Lin},i}\}_{i=1}^N$ denote the vectors of the optimal (training label) and estimated holding forces, respectively. In the above equation, $\ddot{\mathbf{Y}} \in \mathbb{R}^{M\times N}$ is the matrix of input training data, containing absolute values of $M$ acceleration measurements for $N$ decision intervals.

Considering the $L_2$-norm in (7), the approach can be simplified to a least-squares problem. For limited acceleration data, we can find the closed-form solution in a computationally efficient manner. In practice, $\ddot{\mathbf{Y}}$ is a tall matrix that can be constructed by down-sampling the measurement data set for each decision interval. The solution of the least-squares problem in this case is given by

$$\boldsymbol{\theta} = \left(\ddot{\mathbf{Y}}^\intercal \ddot{\mathbf{Y}}\right)^{-1} \ddot{\mathbf{Y}}^\intercal \mathbf{F}^{\text{opt}}. \tag{8}$$

If the input samples in the least-squares problem are not selected sufficiently distinct from each other, $\ddot{\mathbf{Y}}^\intercal \ddot{\mathbf{Y}}$ in (8) may be close to being singular, causing numerical problems. In addition, the formulation in (7) may lead to overfitting and relatively large norms for the estimator $\boldsymbol{\theta}$. In the case of overfitting, the linear estimator fits well to the training acceleration data but performs poorly for unseen acceleration waveforms.

To keep the size of the estimator's parameters sufficiently small and to avoid possible overfitting, we can add a regularization term to (7) as follows:

$$\underset{\boldsymbol{\theta}}{\text{minimize}} \quad \|\mathbf{F}^{\text{opt}} - \mathbf{F}^{\text{lin}}\| = \|\mathbf{F}^{\text{opt}} - \boldsymbol{\theta}^\intercal \ddot{\mathbf{Y}}\| + \lambda \|\boldsymbol{\theta}\| \tag{9}$$

where $\lambda$ is the regularization constant introducing a tradeoff between the minimization of the estimation error and that of the $L_2$-norm of the estimator vector.

The optimization in (9) is equivalent to solving a maximum likelihood problem with *a priori* distribution where the parameters are sampled from a zero-mean Gaussian distribution, also known as maximum a posteriori (MAP) estimation [30]. Using Bayesian linear regression (BLR), one can have a broader view of the concept of parameter prior. In addition, instead of seeking a point-estimate of $\boldsymbol{\theta}$, BLR can evaluate the holding force estimation performance for a distribution of linear estimator functions. Here, we assume that the estimator parameters are drawn from a Gaussian distribution, i.e.,

$$p(\boldsymbol{\theta}) = \mathcal{N}(m_0, S_0)$$

where $m_0$ and $S_0$ denote the mean and variance of the distribution. Also, the estimated holding forces are assumed to be drawn from a Gaussian distribution such that

$$p\left(\hat{F}^{\text{Lin},i} | |\ddot{\mathbf{y}}|^{\boldsymbol{i-1}}, \boldsymbol{\theta}\right) = \mathcal{N}\left(\boldsymbol{\theta}^\intercal |\ddot{\mathbf{y}}|^{i-1}, \sigma^2\right)$$

where $\sigma^2$ denotes the measurement noise variance. Given this assumption, information about the distribution of the estimator parameters can be updated. This posterior over the parameters is obtained using the Bayes theorem as

$$p\left(\boldsymbol{\theta} | \ddot{\mathbf{Y}}, \mathbf{F}^{\text{opt}}\right) = \frac{p\left(\mathbf{F}^{\text{opt}} | \ddot{\mathbf{Y}}, \boldsymbol{\theta}\right) p(\boldsymbol{\theta})}{p\left(\mathbf{F}^{\text{opt}} | \ddot{\mathbf{Y}}\right)}.$$

The following theorem provides the general form of the posterior over the parameters.

*Theorem 1 [30, Th. 9.1]:* Given Assumption 1, the parameter posterior can be computed as

$$\begin{aligned} p\left(\boldsymbol{\theta} | \ddot{\mathbf{Y}}, \mathbf{F}^{\text{opt}}\right) &= \mathcal{N}(\boldsymbol{\theta} | m_N, S_N) \\ S_N &= \left(S_0^{-1} + \sigma^{-2} \ddot{\mathbf{Y}}^\intercal \ddot{\mathbf{Y}}\right) \\ m_N &= S_N\left(S_0^{-1} m_0 + \sigma^{-2} \ddot{\mathbf{Y}}^\intercal \mathbf{F}^{\text{opt}}\right). \end{aligned}$$

Having found the updated estimator parameters, the predictive distribution (posterior) for an unseen acceleration data can be obtained as

$$p\left(\hat{F}^{\text{lin},*}|\ddot{\mathbf{Y}}, \mathbf{F}^{\text{opt}}, \ddot{\mathbf{y}}^*\right) = \int p\left(\hat{F}^{\text{lin},*}|\ddot{\mathbf{y}}^*, \boldsymbol{\theta}\right) p\left(\boldsymbol{\theta}|\ddot{\mathbf{Y}}, \mathbf{F}^{\text{opt}}\right) \mathbf{d}\boldsymbol{\theta}$$
$$= \mathcal{N}\left(\hat{F}^{\text{lin},*}||\ddot{\mathbf{y}}^*|^\top \boldsymbol{\theta}, |\ddot{\mathbf{y}}^*|^\top S_N |\ddot{\mathbf{y}}|^* + \sigma^2\right).$$

*Remark 3:* As discussed in Section II-B, the parameterized policy $\pi_{\boldsymbol{\theta}}$ utilizes the acceleration sample vector $\ddot{\mathbf{y}}^i$ to estimate the electrostatic holding force. The acceleration vector $\ddot{\mathbf{y}}^i$ contains acceleration samples with either positive or negative signs. If the signed values of the acceleration data are employed to learn the parameters of the estimation mapping $\pi_{\boldsymbol{\theta}}$, the learning parameters may not necessarily converge to a stationary value. This leads to large errors in the estimated values of the holding force. Hence, for the linear estimation approach, the magnitude of acceleration samples is utilized.

### B. Estimation Using Multi-Armed Bandit Approach

Given the real-time data processing in the adaptive estimator, one can use a MAB approach as in [26]. Let $F^{\text{MAB},i} \in \mathcal{F}$ denote the estimated holding force at the $i$th decision interval by this approach. The knowledge about the power distribution resulting from a specific holding force is updated after each decision interval. Denote $P^i(F^{\text{MAB},i})$ as the harvested power at the $i$th decision interval as a function of a specific value of the holding force. The expected harvested power for each holding force value is defined as

$$\bar{P} = \mathbb{E}\left[P^i\left(F^{\text{MAB},i}\right)\right] \tag{10}$$

where the expectation in (10) is taken with respect to all decision intervals. The optimal policy is to always select the holding force with the largest expected reward. To this end, this approach initially selects different holding forces to observe and explore their associated harvested power. With sufficient observations, the near-optimal holding force is selected by exploiting the previously collected information. Therefore, one key aspect of such approach is the tradeoff between exploration and exploitation. A variety of algorithms are developed in the literature to tackle such problems in the MAB approach [27], [28].

For our EH maximization problem, MAB algorithms with low computational effort are more favorable. Therefore, in this article, we select the upper confidence bound (UCB) algorithm (Algorithm 1) for estimating the holding force.

### C. Min–Max-Based Adaptive Approach

Considering the optimization problem (3), let $\ddot{y}^{i+}_{\max}$ and $\ddot{y}^{i-}_{\max}$ denote the maximum absolute value of the positive and negative lobes of the acceleration waveform during the $i$th decision interval, respectively. To harvest energy from the acceleration waveform during the $i$th decision interval, the optimal value of the electrostatic force must satisfy the following condition:

$$\frac{F^{i,\Delta}}{m} < \min\left\{\ddot{y}^{i+}_{\max}, \ddot{y}^{i-}_{\max}\right\}. \tag{11}$$

**Algorithm 1** Estimation of the Holding Force With UCB

**Input:** The decision set $\mathcal{F} = \{F_k\}_{k=1}^{10}$, the number of decision intervals $N$, the confidence value $c$, the set of the average collected power of all actions $\{\bar{P}_k\}_{k=1}^{10}$, and the set of occurrences of each actions $\{N_k\}_{k=1}^{10}$

**Output:** Estimated holding force $F^{\text{MAB},i}$

Initialize $\{\bar{P}_p\}_{p=1}^{10} = 0$
Initialize $\{N_k\}_{k=1}^{10} = 0$
**for** $i = 1, \ldots, 10$ **do**
  Select the $i$th action $F^{\text{MAB},i} = F_i$
  Evaluate the harvested power $P^i(F^{\text{MAB},i})$
  $\bar{P}^i = E^i(F^{\text{MAB},i})$
  $N_i \leftarrow N_i + 1$
**end for**
**for** $i = 11, \ldots, N$ **do**
  $F^{\text{MAB},i} = \text{argmax}\, \bar{P}_k + c\sqrt{\frac{\log(i)}{N_k}}$
  Evaluate the harvested power $P^i(F^{\text{MAB},i})$
  $\bar{P}^i = E^i(F^{\text{MAB},i})$
  $N_i \leftarrow N_i + 1$
**end for**

The above inequality implicitly indicates that the electrostatic force must be sufficiently small to make a full flight between the two plates of the CFPG. In other words, the following condition should be taken into account:

$$\int_{t_i}^{t_f} \int_{t_i}^{t} \ddot{z} \mathrm{d}\tau \mathrm{d}t \geq 2Z_l \tag{12}$$

where $\ddot{z} = (F^{i,\Delta}/m) - \ddot{y}^i$ and $t_i$ and $t_f$ denote the initial and final times of the flight, respectively. Motivated by this observation, Algorithm 2 is proposed to estimate the value of the electrostatic force (i.e., $F^{\text{MM}}$).

To solve optimization problem (3), Algorithm 2 detects the zero-crossings of the acceleration waveform. Then, between each two zero-crossings, the maximum value of the acceleration waveform is obtained. These values are collected in $\mathcal{A}^+$ and $\mathcal{A}^-$ as two lists corresponding to positive and negative portions of the acceleration waveform. Let $\bar{\mathcal{A}}^+$ and $\bar{\mathcal{A}}^-$ denote the average of each list. To account for the full-flight condition in (12), we consider a force margin $F_{\text{marg}}$. Then, the holding forces associated with the positive and negative portions of the acceleration waveform are estimated as $m\bar{\mathcal{A}}^+ - F_{\text{marg}}$ and $m\bar{\mathcal{A}}^- - F_{\text{marg}}$, respectively. Finally, condition (11) gives the electrostatic force as the minimum of the two estimated holding forces and the acceleration lists $\mathcal{A}^+$ and $\mathcal{A}^-$ are reset to empty values.

## IV. Acceleration Data Acquisition

To evaluate our proposed power maximization methodologies and obtain a realistic measure of the harvested power, we conducted various physical experiments to acquire human acceleration data. The following sections describes data acquisition and calibration processes that we have used to prepare a sufficiently diverse data set of human motion acceleration.

**Algorithm 2** Min–Max-Based Algorithm

**Input:** Acceleration samples $\ddot{y}$, decision interval length $\Delta$, acceleration sampling frequency $f_s$, the decision set $\mathcal{F}$, force margin $F_{\mathrm{marg}}$, total CFPG execution time $T$, proof mass $m$

**Output:** $F^{\mathrm{MM},i}$

**Variables**
    *zCross*, list of zero-crossing acceleration samples
    Initially empty lists of acceleration $\mathcal{A}^+$ and $\mathcal{A}^-$
    $k$ and $i$ (acceleration sample and decision interval counters, respectively)
**end Variables**
$F^{1,\Delta} \leftarrow \min \mathcal{F}$
$k \leftarrow 2$
**while** $t[k] < T$ **do**
    **if** $\ddot{y}[k]\ddot{y}[k-1] < 0$ **then**
        Append $k$ to *zCross*
    **end if**
    $indx1 \leftarrow zCross(end-1)$, $indx2 \leftarrow zCross(end)$
    **if** $\ddot{y}[indx1 : indx2]$ is a positive array **then**
        append $\max(\mathrm{abs}(\ddot{y}[indx1 : indx2]))$ to $\mathcal{A}^+$
    **else**
        append $\max(\mathrm{abs}(\ddot{y}[indx1 : indx2]))$ to $\mathcal{A}^-$
    **end if**
    **if** $\mathrm{mod}(k, f_s\Delta) = 0$ **then**
        $i \leftarrow i+1$
        $F^{i,\Delta^+} \leftarrow \mathrm{argmin}_{F\in\mathcal{F}} |F - (m\bar{\mathcal{A}}^+ - F_{\mathrm{marg}})|$
        $F^{i,\Delta^-} \leftarrow \mathrm{argmin}_{F\in\mathcal{F}} |F - (m\bar{\mathcal{A}}^- - F_{\mathrm{marg}})|$
        $F^{\mathrm{MM},i} = \min\{F^{i,\Delta^+}, F^{i,\Delta^-}\}$
        Empty $\mathcal{A}^+$ and $\mathcal{A}^-$
    **end if**
    $k \leftarrow k+1$
**end while**

### A. Data Acquisition

To collect acceleration data from the human body motions, the X16-mini triaxial accelerometer made by Gulf Coast Data Concepts, LLC[1] has been used in this study. The dimensions of this device are $51\times25\times13$ mm$^3$. It is small enough to be comfortably placed at various locations on the body and collect data. Body acceleration data is measured along three orthogonal axes. The measurement samples are time-stamped and stored in the device for later retrieval. The sampling rate of the device can be selected to be 12, 25, 50, 100, 200, 400, or 800 Hz. Data are collected from various daily physical activities such as walking, jogging, sit-ups, roping, weight exercises and general random movements of hand and shoulder.[2] Data from each activity are collected for 5 min with the accelerometer attached on the volunteers' wrist, biceps, leg, and chest. To account for changes in the frequency and amplitude of the acceleration waveform, we conducted physical experiments with three intensity levels (slow, moderate, and intense) using ten volunteers. In total, we acquired 144 000 s of acceleration data. Fig. 5 shows a sample twenty-second acceleration waveform for walking in moderate intensity with the accelerometer attached to the wrist.

[1]Commercial products mentioned in this article are merely intended to foster research and understanding. Such identification does not imply recommendation or endorsement by the National Institute of Standards and Technology.

[2]The experiments were conducted according to the research ethics regulations under the approval number 30013664 at Concordia University and ITL-2021-0273 at NIST.

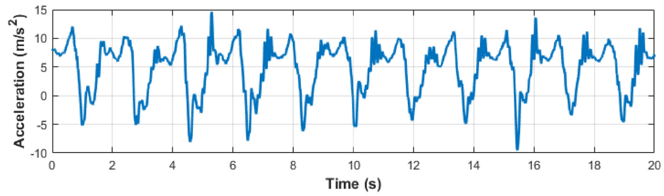


Fig. 5. Acceleration waveform during walking at moderate speed with the accelerometer attached to the wrist.

*Remark 4:* For analysis and performance evaluation of the proposed methodologies in this article, we have chosen the acceleration data in the $z$ axis; however, similar results were observed using data from other axes as well.

*Remark 5:* The range and sampling frequency of the X16-mini triaxial accelerometer is completely sufficient for capturing the human motion data. Other accelerometers with a higher range or sampling frequency will also provide the same raw acceleration data for the purpose of this research. However, the preprocessing step to remove potential biases in the measurement data could slightly change from one accelerometer to another.

The data acquisition process described here is based on potential wearable sensor locations on the body surface. As can be imagined, it is not possible to do similar physical experiments with the accelerometer placed at possible implant locations inside the body. However, it is reasonable to assume that the accelerations applied to an implant and a wearable sensor are almost identical if the wearable device is placed closest to the implant on the surface of the body. The movements of the body part (with the implant) would apply the same acceleration to the implant and the closest wearable sensor on the surface. This would be the case as long as the accelerometer is tightly fixed to the body surface and does not experience additional motion relative to the human body during data acquisition. Therefore, we expect the results obtained in this article can also be applied to implant applications.

### B. Accelerometer Calibration

The raw acceleration data are usually subject to various types of noise and bias. Here, we describe a method to calibrate the measurement data from the accelerometer in order to improve its accuracy. When the accelerometer is stationary, the gravity could impact the measurements. The axis that is perpendicular to the ground senses the constant value of 1g (due to earth gravity) while the other two axes should measure a value of zero. The combined effects of bias, scaling, and cross-axis coupling on the accelerometer output data can be observed by the following procedure. In consecutive time intervals, the static accelerometer is rolled in such a way that first the $z$ axis (and then $y$ and finally $x$) is perpendicular to the ground in order to sense the full impact of gravity in the

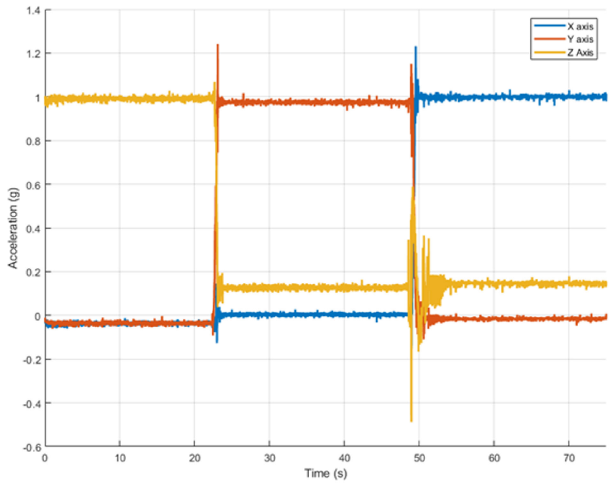


Fig. 6. Accelerometer output data while the device is laid on the ground along $x$, $y$, and $z$ axes.

TABLE I
CALIBRATION PARAMETERS FOR THE ACCELEROMETER

| | | | | | |
|---|---|---|---|---|---|
| $\Lambda_{11}$ | 1.0428 | $\Lambda_{22}$ | 1.0072 | $\mu_1$ | -0.1314 |
| $\Lambda_{12}$ | 0.0043 | $\Lambda_{23}$ | -0.0069 | $\mu_2$ | -0.3268 |
| $\Lambda_{13}$ | -0.0210 | $\Lambda_{33}$ | 0.8230 | $\mu_3$ | 1.3532 |

direction of each axis. Measurement data along each axis for our accelerometer is shown in Fig. 6. To account for scale factors and bias, the following model for triaxial accelerometer is utilized [24]:

$$\tilde{\boldsymbol{a}} = \boldsymbol{\Lambda}\boldsymbol{a} + \boldsymbol{\mu} \tag{13}$$

where $\boldsymbol{a}, \tilde{\boldsymbol{a}} \in \mathbb{R}^3$ denote, respectively, the actual and the measured acceleration vectors along three axes. The matrix $\boldsymbol{\Lambda} \in \mathbb{R}^3$ represents the scaling and cross-axis coupling effects, and $\boldsymbol{\mu} \in \mathbb{R}^3$ is the bias vector. To obtain the exact acceleration vector, (13) is rewritten as

$$\boldsymbol{a} = \boldsymbol{\Lambda}^{-1}(\tilde{\boldsymbol{a}} - \boldsymbol{\mu}).$$

It is desired to calibrate the accelerometer and find the matrix $\boldsymbol{\Lambda}$ and bias vector $\boldsymbol{\mu}$. Considering symmetry in the cross-axis coupling effects, let (13) be rewritten as

$$\tilde{\boldsymbol{a}} = \boldsymbol{A}\boldsymbol{X} \tag{14}$$

where $\boldsymbol{A} \in \mathbb{R}^{3\times 9}$ is a matrix consisting of the elements of the actual acceleration measurements $\boldsymbol{a}$ and

$$\boldsymbol{X} = [\Lambda_{11} \quad \Lambda_{12} \quad \Lambda_{13} \quad \Lambda_{22} \quad \Lambda_{23} \quad \Lambda_{33} \quad \mu_1 \quad \mu_2 \quad \mu_3]^\intercal.$$

One way to obtain the calibration matrix is to collect multiple acceleration measurements for the accelerometer in a stationary mode. Considering $\nu$ acceleration samples, (14) can be expressed in the augmented form as

$$\tilde{\boldsymbol{A}} = \boldsymbol{\Gamma}\boldsymbol{X}$$

where $\boldsymbol{\Gamma} = [\boldsymbol{A}_1^\intercal, \ldots, \boldsymbol{A}_\nu^\intercal]^\intercal$ and $\tilde{\boldsymbol{A}} = [\tilde{\boldsymbol{a}}_1^\intercal, \ldots, \tilde{\boldsymbol{a}}_\nu^\intercal]^\intercal$. For the accelerometer utilized in this study, the calibration parameters were obtained by solving a least-squares problem and the result is reported in Table I.

TABLE II
COMPARISON OF THE HARVESTED POWER (mW) FOR DIFFERENT DECISION SETS DEFINED BY $\delta_F$ AND $F_{\max}$

| $\delta_F$ (mN) \ $F_{\max}$ (mN) | 10 | 20 | 30 |
|---|---|---|---|
| 0.1 | 2.98 | 3.05 | 3.15 |
| 0.25 | 2.9 | 2.98 | 3.05 |
| 0.5 | 2.84 | 2.91 | 2.96 |
| 1 | 2.76 | 2.85 | 2.89 |

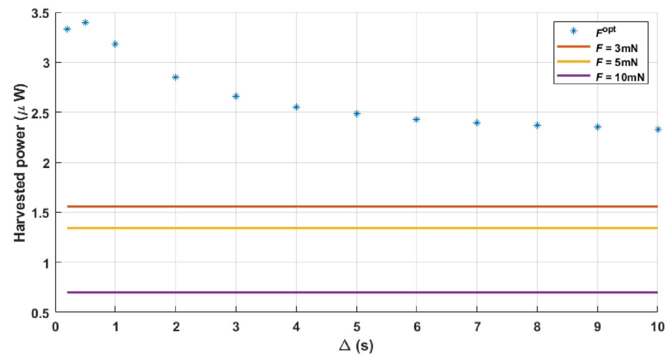


Fig. 7. Comparison of the harvested power for different decision intervals with $F^{\text{opt}}$ and constant holding force $F = 3$, 5, 10 mN.

## V. OPTIMAL PARAMETER SELECTION

In this section, we study the impact of the decision set and the decision interval on the harvested power of the micro-generator.

### A. Impact of the Decision Set

Consider the decision set as defined in (6) with $F_{\min} = 1$ mN, $F_{\max} \in \{10, 20, 30\}$ mN and $\delta_F \in \{0.1, 0.25, 0.5, 1\}$ mN. These values will result in twelve different candidate decision sets. Table II demonstrates the harvested power resulting from each of the candidate decision sets using the offline optimization (5) averaged over acceleration data from various activities discussed in the previous section. As observed, the decision set with the largest range and smallest discretization step offer approximately 13.9% more harvested power compared to the set with the smallest range and largest discretization step (which is approximately thirty times smaller in size). The increase in the harvested power is achieved at the cost of additional computational complexity to estimate the holding force from a larger decision set. Hence, for lower computational cost, the candidate decision set with the smallest range and largest discretization step is selected to evaluate the performance of our proposed adaptive algorithms, i.e., $\mathcal{F} = \{1, \ldots, 10\}$ mN. For the simplicity of notation, we also represent the decision set as $\mathcal{F} = \{F_k\}_{k=1}^{10}$, where $F_k = k$ mN, $k \in \mathbb{N}_{10}$.

### B. Impact of the Decision Interval

The length of the decision interval is another parameter that can affect the average harvested power in (3) and (5). To get a better understanding of this impact, Fig. 7 shows the average harvested power for different values of $\Delta$ and the acceleration waveform resulting from the random movement of the hand. The average power in Fig. 7 has been obtained using the offline optimization (5). For comparison, the average power using several constant values of the electrostatic force (i.e., $F = 3$, 5 and 10 mN) has also been plotted. As $\Delta$ increases, the result of the adaptive optimization (5) converges to the optimal constant electrostatic force, as expected. For the example in Fig. 7, this optimal value is 2 mN. The harvested power for this constant holding force will be almost identical to the power generated through offline optimization (5) for $\Delta > 2000$ s.

As expected, the smaller values of the decision interval result in higher harvested power. For example, compared to the optimal constant holding force, a gain of about 130% is observed for $\Delta = 0.5$ s. It should be noted that the value of the optimal constant holding force cannot be obtained without prior knowledge of the whole acceleration waveform. When other constant values are used for the holding force, the possible gain in the harvested power can be much more. For example, a gain of about 400% is observed in Fig. 7 for $F = 10$ mN and $\Delta = 0.5$ s. For very small values of the decision interval ($\Delta < 0.5$ s), a reduction in the harvested power is observed in Fig. 7. However, this is mainly due to the limitation in the number, range, and resolution of the elements in the decision set. This limitation generally affects the harvested power in any adaptive methodology. This impact is nearly negligible when the size of the decision interval is relatively large. However, shorter decision intervals require finer discretization of the elements of the decision set in order to take advantage of the finer variation of the input acceleration waveform during that interval. Coarse values of the elements in a decision set could over/underestimate the near-optimal value of the holding force, resulting in lower harvested power.

Although choosing smaller decision intervals might seem advantageous, one should consider that smaller intervals are equivalent to more frequent updates of the electrostatic force, requiring more frequent execution of the adaptive optimization algorithm. This will result in more power consumption by the adaptive methodology, reducing the overall output power of the micro-harvester. The tradeoff between smaller decision interval to harvest more power and the decrease in the overall output power due to the consumed energy by the adaptive algorithm module requires further investigation and is outside the scope of this article. The specific technology that is used to implement the adaptive methodology is one of the factors that can impact this tradeoff. Recent technologies such as neuromorphic processors could be a good candidate to implement the proposed adaptive algorithms with ultralow power consumption [12], [13].

The proper choice of the decision interval also depends on the location of the wearable sensor with integrated micro-harvester on the body as well as the nature of the acceleration data and the time spent on the specific daily activities. Selection of this interval is more difficult for activities that involve nonrepetitive motions. Consider the acceleration waveform generated by random movements of the hand shown in Fig. 8. The spectral content of this waveform and its cumulative energy in the frequency domain is also shown in Fig. 9(a) and (b). We conjecture that there is a relationship between the spectral content of the acceleration waveform and the optimal length of the decision interval. Shorter decision intervals could allow an adaptive algorithm to capitalize on high-frequency components of the acceleration waveform and harvest more power, while longer decision intervals limit the algorithm's ability to harvest power from lower frequencies.

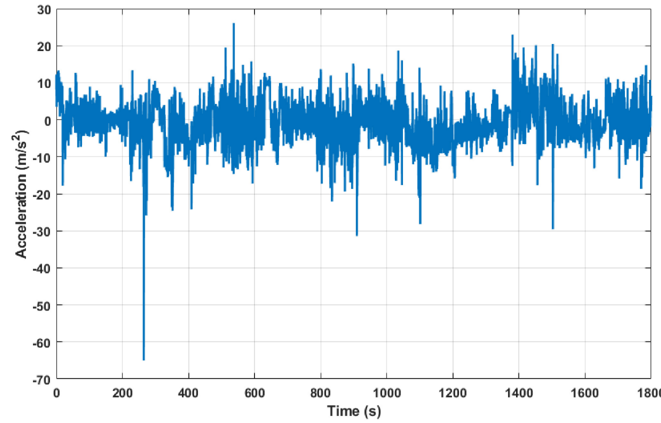


Fig. 8. Acceleration waveform generated by random movements of the hand with the accelerometer on the wrist.

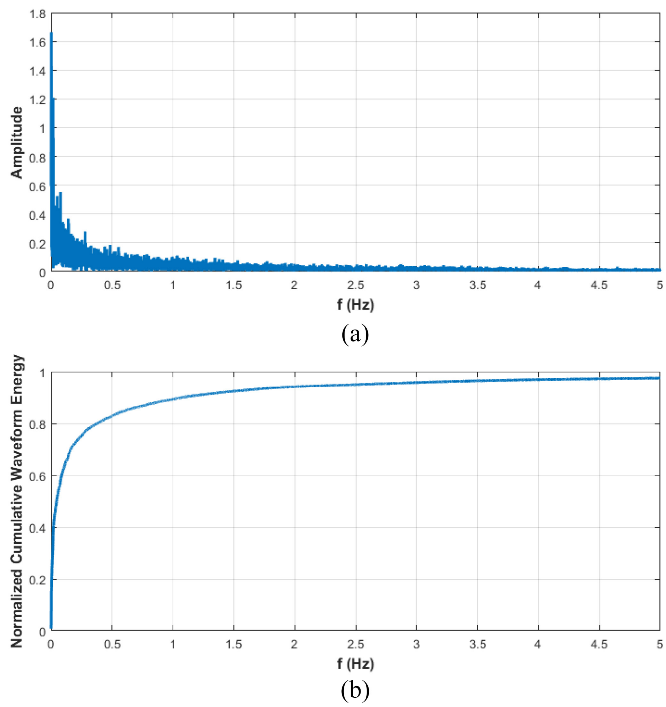


Fig. 9. (a) Amplitude of the frequency components in the acceleration waveform shown in Fig. 8. (b) Corresponding cumulative waveform energy versus frequency.

As observed in Fig. 9, almost 80% of the acceleration waveform energy is included within [0 0.5] Hz interval, which corresponds to a decision interval of 2 s. Considering the tradeoffs mentioned earlier and studying other acceleration waveforms in our data set, we have selected $\Delta = 2$ s to evaluate and compare the performance of the adaptive methodologies.

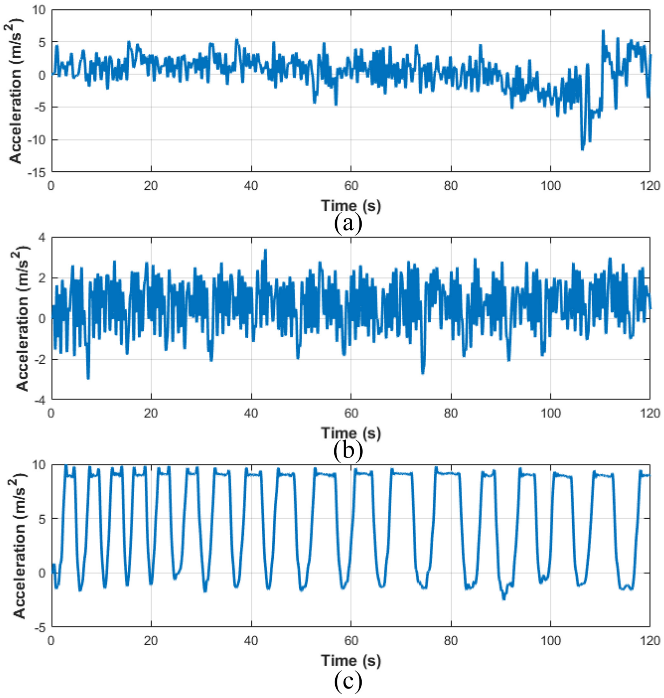


Fig. 10. Acceleration waveforms as test data collected from (a) human arm performing random motions, (b) human chest during sit-ups, and (c) human leg during jogging.

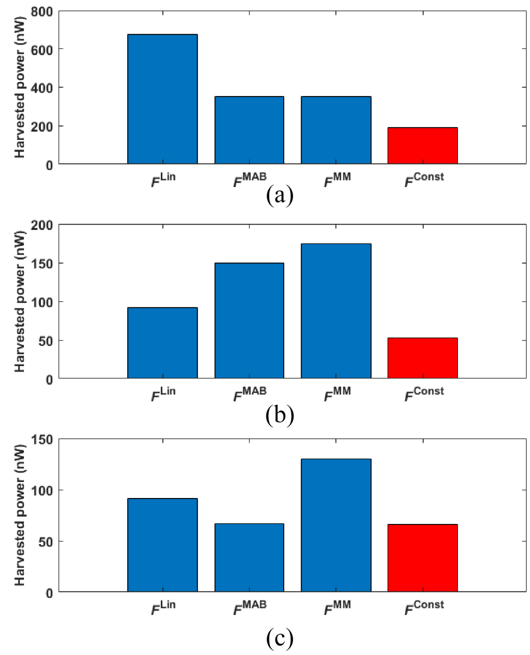


Fig. 11. Comparison of the harvested power using the proposed adaptive methodologies and constant electrostatic force: (a) scenario I; (b) scenario II, and (c) scenario III.

## VI. Performance Evaluation

In this section, the performance of the proposed methodologies are assessed using MATLAB,[3] the mathematical model (1) and experimental data. A CFPG with a proof mass of $m = 1$ g and plates separation of $2Z_l = 1$ mm are considered in our evaluations. From the analysis in Sections V-A and V-B, we consider the decision set $\{1, \ldots, 10\}$ mN and interval $\Delta = 2$ s. For the linear estimator, the acceleration data is down-sampled to 4 Hz, i.e., $\boldsymbol{\theta} \in \mathbb{R}^8$, for a 2-s decision interval. Using this size for the decision interval, the 14 400 seconds of collected data described in the data acquisition section results in 7200 intervals. To learn the parameters of the linear estimator, we select 90% of the collected data for training and the rest is used for validation. For the MAB method described by Algorithm 1, we consider a confidence factor of $c = 0.2$. Also, the force margin in Algorithm 2 is set to $F_{\text{marg}} = 0.5$ mN. We first provide the performance results for three scenarios with the accelerometer attached to different parts of the human body while doing different activities. These scenarios are accelerometer on the: human arm while doing random motions (scenario I); human chest while doing sit-ups (scenario II), and human leg during jogging (scenario III). The corresponding acceleration waveforms are shown in Fig. 10.

Fig. 11 displays the harvested power for each scenario and the adaptive methodologies. For comparison, the average harvested power when a constant holding force is used is also shown for each scenario (i.e., the red bar). As observed, the linear estimator has the best performance for scenario I. However, Algorithm 2 provides more harvested power for scenarios II and III. One reason for the inferior performance of the linear estimator in these two scenarios is the relatively large asymmetry in their corresponding acceleration waveforms (especially in scenario III). In particular, it does not take into account the magnitude of the acceleration data in selecting the holding force, as shown in (11). Compared to the average harvested power using a constant electrostatic force, the best adaptive approach in scenarios I–III offers a gain of about 300%, 400% and 200%, respectively. In scenarios II and III, asymmetry is the most salient feature of the acceleration waveform. Therefore, the min–max-based approach can exploit this asymmetry to outperform the other adaptive methodologies. This feature does not exist in scenario I (i.e., the random motion of the human hand). Therefore, the min–max-based algorithm does not hold any advantage compared to the other methods. On the other hand, the linear method exploits the acceleration intensity in scenario I and outperforms other methods as seen in Fig. 11.

Next, we evaluate the performance of the proposed adaptive approaches for a combination of different human activities over a longer period of time. An acceleration waveform with a duration of 4000 s can be produced by concatenating acceleration data from various individual activities described in Section IV-A. Fig. 12 displays the harvested energy as a result of using our proposed adaptive methodologies on this waveform. For comparison, the average harvested energy using three different constant holding forces is also shown in Fig. 12. Considering the CFPG parameter values as well as the decision set and interval constraints, the upper bound on the extracted

[3]Commercial products mentioned in this article are merely intended to foster research and understanding. Such identification does not imply recommendation or endorsement by the National Institute of Standards and Technology.

TABLE III
COMPARISON OF THE REQUIRED NUMBER OF ELEMENTARY ARITHMETIC OPERATIONS

| | $\pm$ | $\times/$ | $\sqrt{\cdot}$ | $\log(\cdot)$ | $\tanh(\cdot)$ |
|---|---|---|---|---|---|
| Frequency-based approach [21] | 4162 | 1349 | 0 | 0 | 12 |
| DL approach [22] | 162 | 149 | 0 | 0 | 12 |
| MAB approach | 20 | 20 | 1 | 1 | 0 |
| MM approach | 40 | 2 | 0 | 0 | 0 |
| Linear approach | 8 | 7 | 0 | 0 | 0 |

energy (achievable through offline optimization (5)) is also plotted. As observed, among the adaptive approaches, the min–max algorithm performs best, with over 10% more extracted energy compared to the linear estimator. The improvement is due to the fact that this algorithm considers the asymmetry of the acceleration waveform for selecting the proper electrostatic holding force. The min–max adaptive methodology on average generates over 100% more energy compared to the case when a constant holding force is used. This is a promising gain, especially for low-power wearable (or implantable) medical sensors or actuators.

*Remark 6:* Table III provides the required number of arithmetic operations for the proposed methods and those studied in [22] and [23]. The number of operations in functions $\tanh(\cdot)$, $\log(\cdot)$, $\sqrt{\cdot}$ can be obtained by approximating them with their truncated Taylor series expansion (for example, the first ten terms of the series). Let $P_{\text{comp}}$, $P_{\text{avg}}$, $P_{\text{const}}$ and $N_{\text{arith}}$ denote the required average computational power for a single arithmetic operation, the average harvested power of each method for different scenarios, the average harvested power with constant electrostatic force, and the number of the required arithmetic operations by the same method. Depending on the hardware technology employed for the implementation of the algorithms, the use of an adaptive strategy is reasonable as long as

$$P_{\text{avg}} - N_{\text{arith}} \times P_{\text{comp}} > P_{\text{const}}.$$

Therefore, an upper bound for the required computational power of the adaptive module can be estimated as

$$P_{\text{comp}} < \frac{P_{\text{avg}} - P_{\text{const}}}{N_{\text{arith}}}. \tag{15}$$

Compared to a constant force strategy, the use of an adaptive method with $N_{\text{arith}}$ operations is justifiable as long as the required average power satisfies the upper bound in (15).

## VII. CONCLUSION

In this article, three different adaptive approaches were proposed to increase the harvested power in the CFPGs: 1) the linear estimation method; 2) the MAB approach; and 3) the min–max technique. The performance of the proposed methodologies depends on the nature of the acceleration waveform. However, in almost all practical scenarios and on average, there is a noticeable improvement in the harvested kinetic power from the human body motion compared to the case when a constant electrostatic force is used. The additional harvested power could partially supply the required resource to run a low-complexity adaptive algorithm as part of the CFPG architecture. Considering its computational complexity and performance with our acceleration data set, the linear estimator is the best candidate among the studied methodologies.

Knowledge of the exact location of the medical sensor on or inside the body could provide more specific information about the characteristics of the acceleration waveform that an embedded micro-harvester would experience. This information can help to further optimize the adaptive approach with the proper choice of the decision set and interval. Also, the relationship between the best adaptation interval and the spectral content of the acceleration waveform requires additional exploration in future studies.

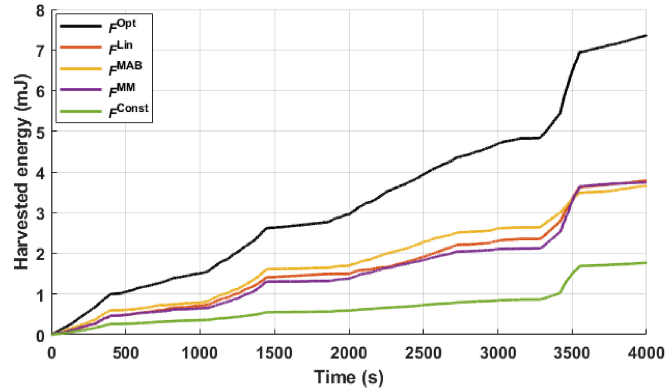


Fig. 12. Comparison of the harvested energy using the proposed adaptive methodologies for a 4000-s acceleration waveform.

## REFERENCES


[1] D. Briand et al., *Micro Energy Harvesting*. Hoboken, NJ, USA: Wiley, Apr. 2015.

[2] M. Magno, D. Kneubuhler, P. Mayer, and L. Benini, "Micro kinetic energy harvesting for autonomous wearable devices," in *Proc. IEEE Int. Symp. Power Electron. Electr. Drives, Autom. Motion (SPEEDAM)*, Jun. 2018, pp. 105–110.

[3] K. Li, Q. He, J. Wang, Z. Zhou, and X. Li, "Wearable energy harvesters generating electricity from low-frequency human limb movement," *Microsyst. Nanoeng.*, vol. 4, no. 1, pp. 1–3, Sep. 2018.

[4] H. C. Koydemir and A. Ozcan, "Wearable and implantable sensors for biomedical applications," *Annu. Rev. Anal. Chem.*, vol. 11, no. 1, pp. 127–146, 2018.

[5] P. Di Barba, L. Fattorusso, and M. Versaci, "A 2D membrane MEMS device model with fringing field: Curvature-dependent electrostatic field and optimal control," *Mathematics*, vol. 9, no. 5, p. 465, Feb. 2021.

[6] P. Mayer, M. Magno, and L. Benini, "Energy-positive activity recognition from kinetic energy harvesting to smart self-sustainable wearable devices," *IEEE Trans. Biomed. Circuits Syst.*, vol. 15, no. 5, pp. 926–937, Oct. 2021.

[7] L. Wang et al., "Overview of human kinetic energy harvesting and application," *ACS Appl. Energy Mater.*, vol. 5, no. 6, pp. 7091–7114, 2022.

[8] P. Gawron, R. M. Wendt, L. Stiglmeier, N. Hangst, and U. B. Himmelsbach, "A review on kinetic energy harvesting with focus on 3D printed electromagnetic vibration harvesters," *Energies*, vol. 14, no. 21, p. 6961, Oct. 2021.

[9] P. D. Mitcheson, T. C. Green, E. M. Yeatman, and A. S. Holmes, "Architectures for vibration-driven micropower generators," *J. Microelectromech. Syst.*, vol. 13, no. 3, pp. 429–440, Jun. 2004.

[10] Y. Khan, A. E. Ostfeld, C. M. Lochner, A. Pierre, and A. C. Arias, "Monitoring of vital signs with flexible and wearable medical devices," *Adv. Mater.*, vol. 28, no. 22, pp. 4373–4395, 2016.

[11] A. Cadei, A. Dionisi, E. Sardini, and M. Serpelloni, "Kinetic and thermal energy harvesters for implantable medical devices and biomedical autonomous sensors," *Meas. Sci. Technol.*, vol. 25, no. 1, Nov. 2013, Art. no. 12003.

[12] M. R. Azghadi et al., "Hardware implementation of deep network accelerators towards healthcare and biomedical application," *IEEE Trans. Biomed. Circuits Syst.*, vol. 14, no. 6, pp. 1138–1159, Dec. 2020.

[13] E. Donati, M. Payvand, N. Risi, R. Krause, and G. Indiveri, "Discrimination of EMG signals using a neuromorphic implementation of a spiking neural network," *IEEE Trans. Biomed. Circuits Syst.*, vol. 13, no. 5, pp. 795–803, Oct. 2019.

[14] P. D. Mitcheson, T. Sterken, C. He, E. M. Kiziroglou, E. M. Yeatman, and R. Puers, "Electrostatic microgenerators," *Meas. Control*, vol. 41, no. 4, pp. 114–119, 2008.

[15] P. D. Mitcheson, "Analysis and optimisation of energy-harvesting microgenerator systems," Ph.D. dissertation, Imperial College London, Univ. London, London, U.K., 2005.

[16] T. Von Buren, P. D. Mitcheson, T. C. Green, E. M. Yeatman, A. S. Holmes, and G. Troster, "Optimization of inertial micropower generators for human walking motion," *IEEE Sensors J.*, vol. 6, no. 1, pp. 28–38, Feb. 2006.

[17] P. D. Mitcheson, "Energy harvesting for human wearable and implantable bio-sensors," in *Proc. IEEE Int. Conf. Eng. Med. Biol.*, Aug. 2010, pp. 3432–3436.

[18] D. Budic, D. Šimunic, and K. Sayrafian, "Kinetic-based micro energy-harvesting for wearable sensors," in *Proc. 6th IEEE Int. Conf. Cogn. Infocommun. (CogInfoCom)*, 2015, pp. 505–509.

[19] N. Yarkony, K. Sayrafian, and A. Possolo, "Energy harvesting from the human leg motion," in *Proc. 8th Int. Conf. Pervasive Comput. Technol. Healthcare*, 2014, pp. 88–92.

[20] M. Dadfarnia, K. Sayrafian, P. D. Mitcheson, and J. S. Baras, "Maximizing output power of a CFPG micro energy-harvester for wearable medical sensors," in *Proc. 4th Int. Conf. Wireless Mobile Commun. Healthcare-Transforming Healthcare Through Innov. Mobile Wireless Technol. (MOBIHEALTH)*, 2014, pp. 218–221.

[21] M. Roudneshin, K. Sayrafian, and A. G. Aghdam, "A machine learning approach to the estimation of near-optimal electrostatic force in micro energy-harvesters," in *Proc. IEEE Int. Conf. Wireless Space Extreme Environ. (WiSEE)*, 2019, pp. 71–75.

[22] M. Roudneshin, K. Sayrafian, and A. G. Aghdam, "Adaptive estimation of near-optimal electrostatic force in micro energy-harvesters," in *Proc. IEEE Int. Conf. Control Technol. Appl. (CCTA)*, 2020, pp. 782–786.

[23] M. Roudneshin, K. Sayrafian, and A. G. Aghdam, "Maximizing harvested energy in coulomb force parametric generators," in *Proc. Amer. Control Conf. (ACC)*, Jun. 2022, pp. 1801–1807.

[24] P. Batista, C. Silvestre, P. Oliveira, and B. Cardeira, "Accelerometer calibration and dynamic bias and gravity estimation: Analysis, design, and experimental evaluation," *IEEE Trans. Control Syst. Technol.*, vol. 19, no. 5, pp. 1128–1137, Sep. 2011.

[25] K. P. Murphy, *Machine Learning: A Probabilistic Perspective*. Cambridge, MA, USA: MIT Press, Sep. 2012.

[26] R. S. Sutton and A. G. Barto, *Reinforcement Learning: An Introduction*. Cambridge, MA, USA: MIT Press, Nov. 2018.

[27] D. Bouneffouf, I. Rish, and C. Aggarwal, "Survey on applications of multi-armed and contextual bandits," in *Proc. IEEE Congr. Evol. Comput. (CEC)*, Jul. 2020, pp. 1–8.

[28] L. Zhou, "A survey on contextual multi-armed bandits," Aug. 2015, *arXiv:1508.03326*.

[29] C. Cepnik, R. Lausecker, and U. Wallrabe, "Review on electrodynamic energy harvesters—A classification approach," *Micromachines*, vol. 4, no. 2, pp. 168–196, 2013.

[30] M. P. Deisenroth, A. A. Faisal, and C. S. Ong, *Mathematics for Machine Learning*. Cambridge, U.K.: Cambridge Univ. Press, Apr. 2020.


**Masoud Roudneshin** (Member, IEEE) received the B.S. and M.S. degrees in mechanical engineering from Sharif University of Technology, Tehran, Iran, in 2014 and 2016, respectively, and the Ph.D. degree in electrical engineering from Concordia University, Montreal, QC, Canada, in 2022.

He is currently a Research Scientist with Traxara Robotics, Montreal. His research interests span optimization, energy harvesting, control, and robotics.

Dr. Roudneshin was the recipient of the Merit-Based Award for the B.S. dual major program of mechanical and aerospace engineering at Sharif University of Technology. He is also a recipient of the Mitacs Accelerate Fellowship and Concordia University Graduate Award.

**Kamran Sayrafian** (Senior Member, IEEE) received the M.S. degree in electrical and computer engineering from Villanova University, Villanova, PA, USA, in 1992, and the Ph.D. degree in electrical and computer engineering from the University of Maryland, College Park, MD, USA, in 2000.

He is currently a Senior Scientist with the Information Technology Laboratory, National Institute of Standards and Technology (NIST), Gaithersburg, MD, USA, where he leads a strategic program related to the application of the Internet of Things (IoT) in healthcare. He has also been an affiliate Associate Professor with Concordia University, Montreal, QC, Canada, since 2016. Prior to joining NIST, he was the Co-Founder of Zagros Networks, Inc., a fabless semiconductor company based in Rockville, MD, USA, where he served as the President and a Senior Member of the architecture team. He is the co-inventor/inventor of four U.S. patents. He has published over 120 conference and journal papers, and book chapters. His current research interests include body area networks, micro energy harvesting, automatic exposure notification, and IoT technology in healthcare.

Dr. Sayrafian has been the recipient of the IEEE PIMRC 2009, the SENSORCOMM 2011, the IEEE CSCN 2018, and the IEEE EuCNC 2019 Best Paper Awards. He was a major contributor to the development of the IEEE802.15.6 international standard on Body Area Networks; and the recipient of the 2015 U.S. Department of Commerce Bronze Medal for his contribution to this emerging field. He is the Co-Chair of the Vertical Track on Health and Well-Being at the COST CA20120 "Intelligence-Enabling Radio Communications for Seamless Inclusive Interactions." He has served as the Technical Program Committee and Executive Co-Chair for the IEEE PIMRC 2014 and an Organizer of several other IEEE ComSoc Conferences and international workshops focused on the applications of wireless communication in healthcare. He was also a member of the Editorial Board of the *IEEE Wireless Communication Magazine* from 2016 to 2020. In 2014, he also served as the U.S. Embassy Science Fellow in Croatia. He is a Fellow of the Washington Academy of Sciences.

**Amir G. Aghdam** (Fellow, IEEE) received the Ph.D. degree in electrical and computer engineering from the University of Toronto, Toronto, ON, Canada, in 2000.

He is currently a Professor with the Department of Electrical and Computer Engineering, Concordia University, Montreal, QC, Canada, and an Associate Dean of Graduate Studies with Gina Cody School of Engineering and Computer Science. He was a Visiting Scholar with Harvard University, Cambridge, MA, USA, in the fall of 2015 and was an Associate with the Harvard John A. Paulson School of Engineering and Applied Sciences from September 2015 to December 2016. His research interests include distributed control of interconnected systems.

Dr. Aghdam is the Chair of the Conference Editorial Board of IEEE Control Systems Society, and the Editor-in-Chief of the IEEE SYSTEMS JOURNAL. He served as an Associate Editor for several IEEE journals, including the IEEE TRANSACTIONS ON CONTROL SYSTEMS TECHNOLOGY and IEEE ACCESS. He was a member of the Review Committee for the Italian Research and University Evaluation Agency in 2012–2013 and the Natural Sciences and Engineering Research Council of Canada ECE Evaluation Group in 2014–2016. He was the 2014–2015 President of IEEE Canada and Director (Region 7), IEEE, Inc., and was also a member of the IEEE Awards Board for this period. He was a member of the IEEE Medal of Honor Committee and IEEE MGA Awards and Recognition Committee. He is currently the Chair of the IEEE Medals Council.